A number of rhodium(III) complexes of thiacrown ligands can be reduced to give rhodium(II) species identifiable in solution. Thus controlled potential electrolysis of $Rh(9S_3)_2^{3+}$ ($9S_3$ = 1,4,7-trithiacyclononane) gives $Rh(9S_3)_2^{2+}$ ($g_1 = 2.085$, $g_2 = 2.042$, $g_3 = 2.009$) [82].

2.9 Rhodium(III) complexes

A considerable number of rhodium(III) complexes exist. Their stability and inertness are as expected for a low-spin d^6 ion; any substitution leads to a considerable loss of ligand-field stabilization.

2.9.1 Complexes of O-donors

The yellow acetylacetonate contains octahedrally coordinated rhodium (Rh–O 1.992 Å; O–Rh–O 95.3°) [83].

$$Rh(NO_3)_3 \xrightarrow[pH\,7]{acac^-} Rh(acac)_3$$

The corresponding tri- and hexa-fluoroacetylacetonates may be similarly prepared. The stability of the acetylacetonate is such that not only can it be resolved on passage through a column of D-lactose, but the enantiomers retain their integrity on nitration or bromination.

Extended refluxing of hydrated $RhCl_3$ with excess oxalate leads to the tris complex, the potassium salt crystallizing as orange–red crystals with Rh–O 2.000–2.046 Å.

$$RhCl_3.3H_2O \xrightarrow[reflux,\,6\,h]{aq.\,K_2C_2O_4\,(6\,mol)} K_3Rh(C_2O_4)_3.4\tfrac{1}{2}H_2O$$

$Rh(C_2O_4)_3^{3-}$ was resolved by Werner as the strychnine salt but other ions, such as $Coen_3^{3+}$ and $Niphen_3^{3+}$, have been used more regularly for this [84].

The dinuclear rhodium(II) acetate is described in section 2.8.2; the dinuclear structure is retained on one-electron oxidation, but when ozone is used as the oxidant, a compound with a trinuclear Rh_3O core is formed, analogous to those formed by Fe, Cr, Mn and Ru. (It can also be made directly from $RhCl_3$.)

$$RhCl_3.3H_2O \xrightarrow[2.\,ClO_4^-]{1.\,MeCOOAg} [Rh_3O(O_2CMe)_6(H_2O)_3]^+ClO_4^-$$

$$Rh_2(O_2CMe)_4 \xrightarrow[2.\,ClO_4^-]{1.\,O_3/boiling\,MeCOOH} [Rh_3O(O_2CMe)_6(H_2O)_3]^+ClO_4^-$$

Rhodium forms an EDTA complex isomorphous with the corresponding ones of Ru, Fe, Ga and Cr. In Rh(EDTAH)(H_2O) one carboxylate is protonated and thus the acid is pentadentate, the water molecule completing the octahedron (Figure 2.43).

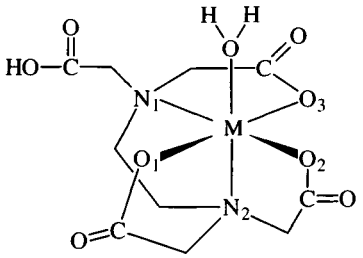

(M = Rh, Ru)

	Rh	Ru
M-OH2	2.096	2.131
M-N1	2.082	2.13
M-N2	1.988	2.038
M-O1	2.001	1.988
M-O2	2.007	2.007
M-O3	2.03	2.06

Figure 2.43 Ruthenium and rhodium EDTA complexes. Comparative bond lengths are given in Table 2.4.

Table 2.4 Bond lengths in M(EDTAH)(H_2O) (M = Ru, Rh) (Å)

	Ru	Rh
$M-OH_2$	2.131	2.096
$M-N_1$	2.130	2.082
$M-N_2$	2.038	1.988
$M-O_1$	1.988	2.001
$M-O_2$	2.007	2.007
$M-O_3$	2.060	2.030

The bond lengths make a more regular octahedron than in the d^5 ruthenium analogue, possibly partly a consequence of the symmetrical electron distribution in the d^6 Rh^{3+} ion (Table 2.4) [85].

2.9.2 Complexes of ammines

Amine complexes are an important class of rhodium(III) complex. Figure 2.44 shows some relationships.

Hexammines

Hexammines are more difficult to prepare than the pentammines, one route to $Rh(NH_3)_6^{3+}$ involving substitution under forcing conditions [86]:

$$[Rh(NH_3)_5Cl]Cl_2 \xrightarrow[100°C\text{ sealed tube}]{NH_3\text{ (aq.)}} [Rh(NH_3)_6]Cl_3$$

It is more convenient to start with the triflate ion $[Rh(NH_3)_5(CF_3SO_3)]^{2+}$ since triflate is a much better leaving group than chloride and is immediately replaced by liquid ammonia [87]. A third route involves acid hydrolysis of the cyanate complex $[Rh(NH_3)_5(NCO)]^{2+}$, which proceeds quantitatively (probably via a carbamic acid complex). Vibrational studies on $Rh(NH_3)_6^{3+}$ assign stretching vibrations as $\nu_1(A_{1g})$ at 514 cm^{-1}, $\nu_2(E_g)$ at 483 cm^{-1} and $\nu_3(T_{1u})$ at 472 cm^{-1} [88].

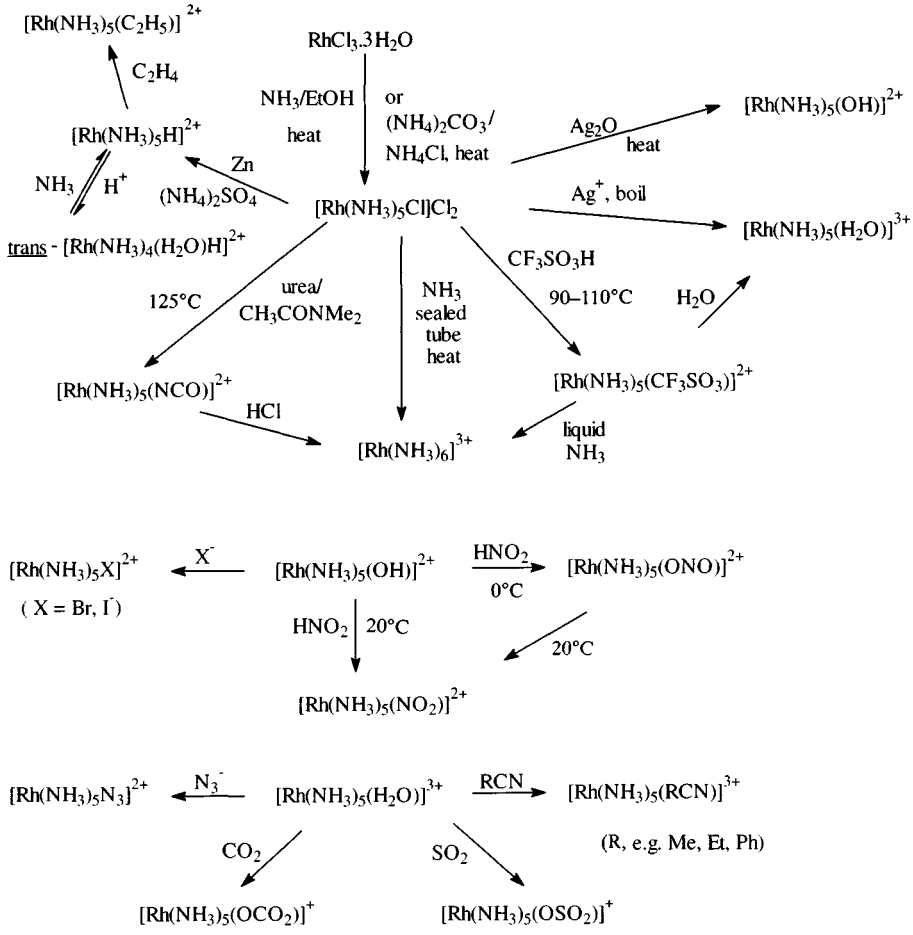

Figure 2.44 Syntheses and reactions of rhodium(III) ammine complexes.

Pentammines

The most important of the pentammines is the chloride $[Rh(NH_3)_5Cl]Cl_2$, prepared by one of two routes [89]:

$$RhCl_3.3H_2O \xrightarrow[EtOH]{NH_3\ (aq.)} [Rh(NH_3)_5Cl]Cl_2$$

The ethanol is implicated in forming a rhodium(I) complex that catalyses the reaction. The second method produces a mixture

$$RhCl_3.3H_2O \xrightarrow[H_2O,\ heat]{(NH_4)_2CO_3/NH_4Cl} [Rh(NH_3)_5Cl]Cl_2 + [Rh(NH_3)_4Cl_2]Cl$$

which is easily separable because the yellow pentammine precipitates while the more soluble tetrammine stays in solution. Other pentammines can be made by metathesis with NaX or by substitution of the aquo complex.

$$[Rh(NH_3)_5(H_2O)]^{3+} \xrightarrow{X^-} [Rh(NH_3)_5X]^{2+} \qquad (X = Cl, Br, I)$$

X-ray diffraction studies on $[Rh(NH_3)_5X]X_2$ (X = Cl, Br) yield Rh–N 2.051–2.061 Å (X = Cl) and 2.052–2.062 Å (X = Br) with Rh–Cl 2.355 Å and Rh–Br 2.491 Å, respectively [90].

The most remarkable pentammine is the hydride $[Rh(NH_3)_5H]^{2+}$ [91], produced by zinc (powder) reduction of the chloropentammine salt. It shows ν(Rh–H) at 2079 cm^{-1} in the IR spectrum (of the sulphate) and the low-frequency hydride NMR resonance at $\delta = -17.1$ ppm as a doublet showing Rh–H coupling (14.5 Hz). Its crystal structure shows the pronounced *trans*-influence of hydride, with the Rh–N bond *trans* to H some 0.17 Å longer than the *cis* Rh–N bond (Figure 2.45) [92].

Kinetic inertness, evidently caused by the electronic configuration, leads to a remarkable unreactivity of the Rh–H bond to hydrolysis. In the absence of air, it is unaffected by ammonia solution: in dilute solution, the ammonia *trans* to hydride is reversibly replaced by water, showing that the hydride has a *trans*-effect parallel to its *trans*-influence.

$$Rh(NH_3)_5H^{2+} + H_2O \Leftrightarrow Rh(NH_3)_4(H)(H_2O)^{2+} + NH_3$$

Both these hydrides insert alkenes and alkynes; the crystal structure of $[Rh(NH_3)_5(C_2H_5)]^{2+}Br_2$ shows the ethyl group has a *trans*-influence comparable to that of the hydride [93].

The hydroxypentammine is a useful starting material for the nitro and nitrito linkage isomers, the nitrito form separating under mild conditions but transforming to the nitro isomer on standing, especially when heated.

$$[Rh(NH_3)_5OH]^{2+}Cl_2 \xrightarrow[12\,M\,HCl\,0°C]{NaNO_2} [Rh(NH_3)_5(ONO)]Cl_2$$

$$\downarrow \text{ stand, heat}$$

$$[Rh(NH_3)_5(NO_2)]Cl_2$$

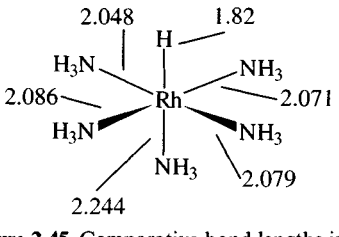

Figure 2.45 Comparative bond lengths in $[Rh(NH_3)_5H]^{2+}$ and $[Rh(NH_3)_5Et]^{2+}$.

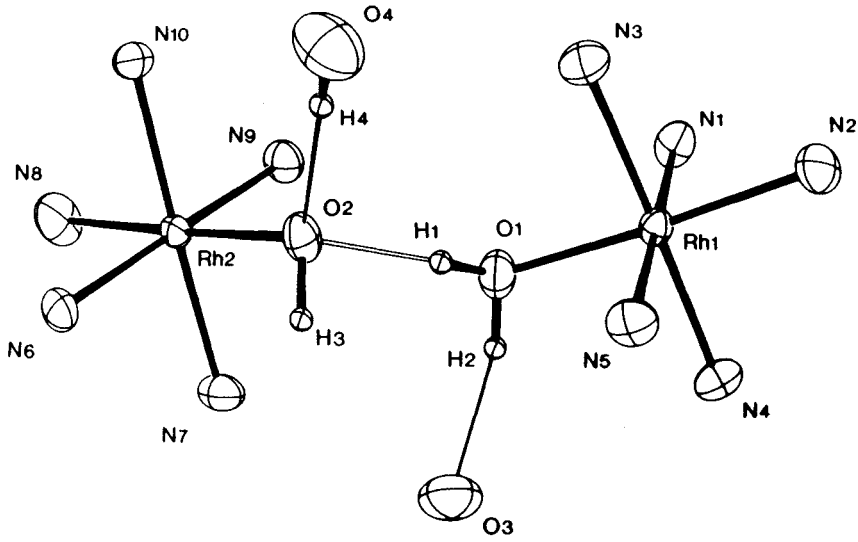

Figure 2.46 The structure of $[(NH_3)_5Rh(H_7O_4)Rh(NH_3)_5]^{5+}$. (Reproduced with permission from *Z. Naturforsch., Teil B*, 1988, **43**, 189.)

$[Rh(NH_3)_5OH]^{2+}$ reacts with $[Rh(NH_3)_5(H_2O)]^{3+}$ to form $[(NH_3)_5Rh(H_7O_4)$-$Rh(NH_3)]^{5+}$ (Figure 2.46) in which there is a μ-H_3O_2 bridge between the coordinated H_2O and OH groups [94].

Tetrammines

A useful route into the tetrammine series starts from the readily available chloropentammine, substitution with oxalate giving the (necessarily) *cis*-tetrammine, conveniently isolable as a perchlorate [95]:

$$Rh(NH_3)_5Cl^{2+} \xrightarrow[120°C,\,14\,h]{Na_2C_2O_4/H_2C_2O_4} [Rh(NH_3)_4(C_2O_4)]^+$$

The oxalate can then be replaced by chloride or bromide:

$$cis\text{-}[Rh(NH_3)_4(C_2O_4)]^+ \xrightarrow{HCl} cis\text{-}[Rh(NH_3)_4Cl_2]^+$$

The *trans*-isomer can be obtained as a second product in the pentammine synthesis, also by

$$[Rh(NH_3)_5H]^{2+} \xrightarrow[2.\,H_2O_2/HCl\,pH\,1]{1.\,KCl\,pH\,6} trans\text{-}[Rh(NH_3)_4Cl_2]^+Cl^-$$

In this reaction, the ammonia *trans* to hydride then the hydride itself are both replaced. In *trans*-$[Rh(NH_3)_4Cl_2]^+Cl^-$, Rh–N is 2.07 Å and Rh–Cl 2.31 Å [96].

Photochemical reactions of rhodium(III) ammines

Though thermally stable, rhodium ammines are light sensitive and irradiation of such a complex at the frequency of a ligand-field absorption band causes substitution reactions to occur (Figure 2.47) [97]. The charge-transfer transitions occur at much higher energy, so that redox reactions do not compete.

Irradiation of solutions of *cis*-$[Rh(NH_3)_4Cl_2]^+$ at 366 nm formed mainly *trans*-$[Rh(NH_3)_4Cl(H_2O)]^{2+}$ with a little *cis*-isomer. *Trans*-$[Rh(NH_3)_4Cl_2]^+$ behaves similarly. The isomeric chloro aqua complexes photochemically interconvert but eventually form a stationary state.

The *cis*/*trans* ratio is the same for both reactions, suggesting a common intermediate. In an important reinvestigation, it was found that *cis*-$[Rh(NH_3)_4Cl(H_2O)]^{2+}$, *cis*-$[Rh(NH_3)_4Cl_2]^+$ and the corresponding *trans*-isomers give the same mixture of 17% *cis*- and 83% *trans*-$[Rh(NH_3)_4Cl(H_2O)]^{2+}$,

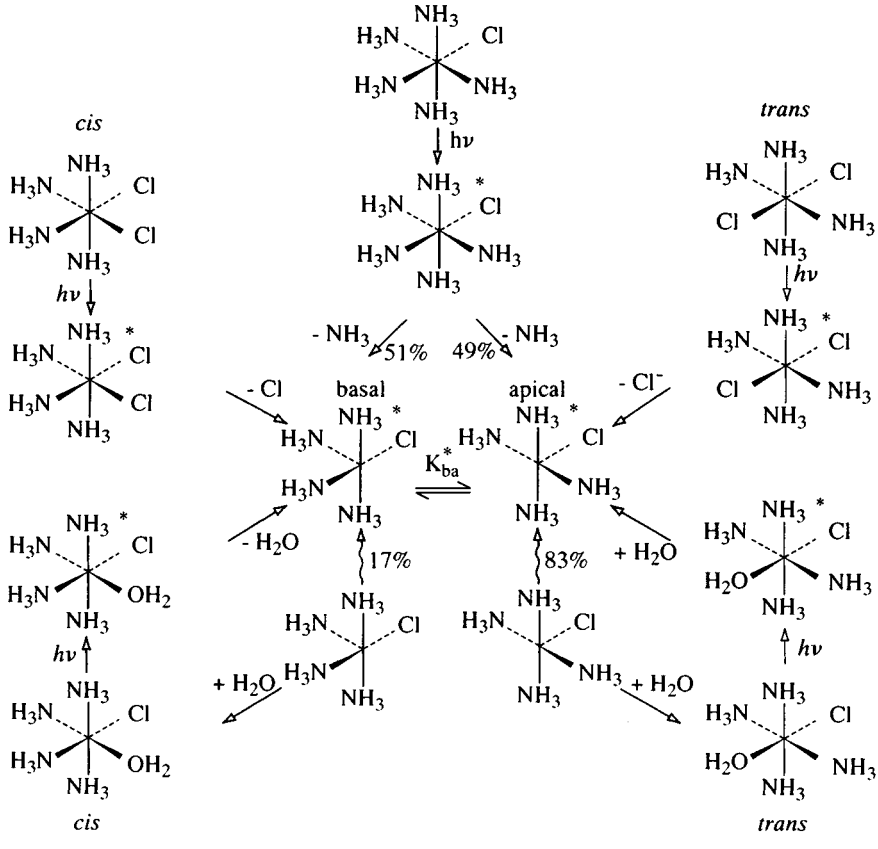

Figure 2.47 The limiting photosubstitution mechanism for rhodium(III) ammine complexes. (Reprinted from *Coord. Chem. Rev.*, **94**, 151, 1989, with kind permission from Elsevier Science S.A., P.O. Box 564, 1001 Lausanne, Switzerland.)

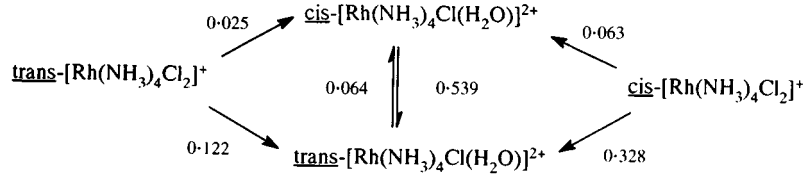

Figure 2.48 Quantum yields for the photolysis of rhodium(III) ammine complexes.

implying that photolysis takes a dissociative pathway leading to a 5-coordinate intermediate that can equilibrate with its isomer before being attacked by a water molecule to give the final $[Rh(NH_3)_4Cl(H_2O)]^{2+}$ ion (Figure 2.48).

Solvent can affect the product yields. $[Rh(NH_3)_5Cl]^{2+}$ tends to lose Cl^- in polar media, but in less polar solvents (MeOH, DMSO) that cannot solvate Cl^- so well, ammine loss predominates. $[Rh(NH_3)_5N_3]^{2+}$ in HCl solution undergoes mainly substitution to give $[Rh(NH_3)_5Cl_2]^+$ and N_2, but other products include $[Rh(NH_3)_5(NH_2OH)]^{3+}$.

2.9.3 Complexes of other N-donors

A range of pyridine complexes can be made [98]

$$\textit{trans}\text{-}Rhpy_4Cl_2^+ \xleftarrow[\text{trace EtOH}]{\text{py}} RhCl_6^{3-} \xrightarrow[\text{py}]{\text{neat}} \textit{fac} \text{ and } \textit{mer}\text{-}RhCl_3py_3$$

Apart from ethanol, other primary alcohols catalyse the formation of the dichloro complex, probably via a rhodium(I) intermediate rather than a rhodium(III) hydride. $Rhpy_4X_2^+$ compounds have anti-bacterial activity.

Though it is not possible to replace the remaining two chlorides in $[Rhpy_4Cl_2]^+$ by pyridine, possibly owing to steric effects, it can be used as a starting material for a number of syntheses. With ammonia it gives $[Rh(NH_3)_5Cl]^{2+}$, and with bidentate amines (en, phen) it gives ions like *trans*-$[Rhen_2Cl_2]^+$ (excess amine leads to $Rhen_3^{3+}$).

Nitrile complexes are synthesized by a variety of routes (Figure 2.49).

$Rh(NO_2)_6^{3-}$ is of some importance in the traditional extraction of rhodium. Impure $RhCl_3$ is neutralized and treated with $NaNO_2$; $Na_3Rh(NO_2)_6$ is soluble under these conditions (though base metals precipitate), but when ammonium chloride is added, $(NH_4)_3Rh(NO_2)_6$ precipitates. The potassium salt is similarly relatively insoluble. All these salts are believed

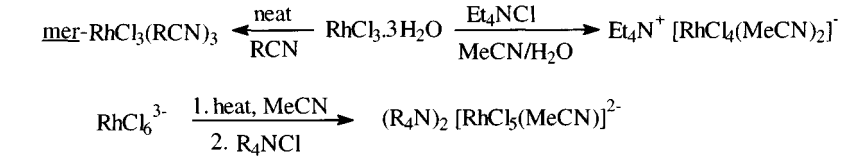

Figure 2.49 Synthesis of rhodium(III) nitrile complexes.

to involve N-bonded NO_2 groups; confirmed (X-ray) for $Na_3Rh(NO_2)_6$ (Rh–N 2.056 Å) [99].

Polydentate N-donors

The synthesis of $Rhen_3^{3+}$, mentioned above, is again accelerated by a trace of ethanol catalyst

$$RhCl_3.3H_2O \xrightarrow[\text{aq. EtOH}]{\text{en}} Rhen_3Cl_3$$

It exists as optical isomers and was first resolved by Alfred Werner. The route to the bis complexes generates the ammine *in situ* and is applicable to other ammines (tren, trien, etc.) yielding principally the *trans*-isomer

$$RhCl_3.3H_2O \xrightarrow[\text{2. 2 equiv. NaOH}]{\text{1. 2 equiv. en HCl reflux}} \textit{trans}\text{-}[Rhen_2Cl]^+Cl^-$$

Entry into the *cis*-diammine system (Figure 2.50) uses the chelating ligand oxalate, as with the ammines; use of $NaBH_4$ as catalyst speeds this up.

The oxalate can be removed by acid hydrolysis. *cis*-$Rhen_2X_2^+$ complexes have also been resolved for X = Cl, NO_2 and $\frac{1}{2}C_2O_4$ [100].

With the more rigid phen and bipy, *cis*-$Rh(L{-}L)_2X_2^+$ can be prepared using ethanol in a reaction reminiscent of the synthesis of $Rhpy_4Cl_2^+$

$$RhCl_3.3H_2O \xrightarrow{\text{L–L/EtOH}} \textit{cis}\text{-}Rh(L{-}L)_2Cl_2^+ \qquad (L{-}L = \text{phen, bipy})$$

$$RhX_6^{3-} \xrightarrow{\text{phen}} Rh(\text{phen})X_4^- \xrightarrow{\text{phen}} \textit{cis}\text{-}Rh(\text{phen})_2X_2^+ \qquad (X = Cl, Br)$$

A recent facile synthesis of $Rh(L{-}L)_3^{3+}$ is:

$$RhCl_3.3H_2O \xrightarrow{AgL_2^+X^-} Rh(L{-}L)_3^{3+}(X^-)_3$$

(X = ClO_4, NO_3; L = phen, bipy).

Like the ammines, rhodium complexes of ligands like bipy and phen have a significant photochemistry. Therefore, on irradiation, solutions of *cis*-$[Rh(L{-}L)_2X(H_2O)]^{2+}$ (X = halogen) gradually convert to *cis*-$[Rh(L{-}L)_2X(H_2O)]^{2+}$, though much more slowly than with the ammines [101].

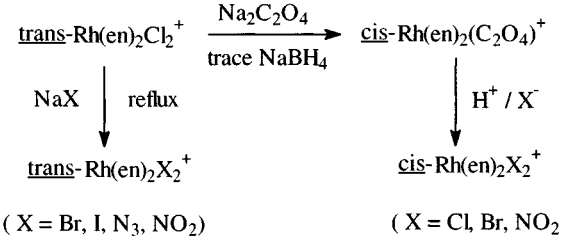

Figure 2.50 Synthesis of rhodium(III) complexes of ethylenediamine.

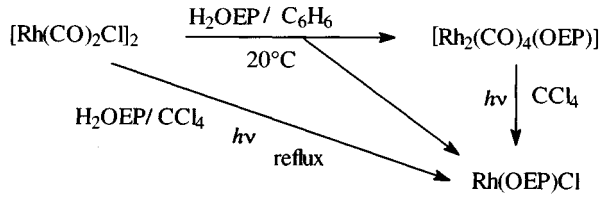

Figure 2.51 Synthesis of rhodium porphyrin complexes.

Macrocycles

Reaction of $[Rh(CO)_2Cl]_2$ with porphyrins (e.g. H_2TPP) leads to Rh(porphyrin)(CO)Cl, which readily lose CO. Some of the chemistry of the octaethylporphyrin complexes [102] is shown in Figures 2.51 and 2.52.

Two forms of the methyl complex have been characterized by X-ray diffraction; the Rh–C distances differ slightly at 1.97 and 2.01 Å, though the sp coordination geometry is the same.

The rhodium(II) compound is a diamagnetic dimer; with oxygen it forms a paramagnetic monomeric O_2 adduct, probably a superoxide complex represented as $(porph)Rh^{3+}O_2^-$.

2.9.4 Complexes of S-donors

The thiocyanate $(Ph_4P)_3[Rh(SCN)_6]$ is S-bonded, with Rh–S 2.372 Å; however, linkage isomers $[Rh(NCS)_n(SCN)_{6-n}]^{3-}$ exist, separable by chromatography [103].

A series of sulphide complexes can be made by refluxing the rhodium trihalide with the appropriate organic sulphide in methanol or ethanol:

$$RhX_3 + 3R_2S \xrightarrow[\text{reflux}]{\text{MeOH}} \textit{mer}\text{-}RhX_3(R_2S)_3$$

(R = Me, Et, Pr; $R_2 = (CH_2)_4$).

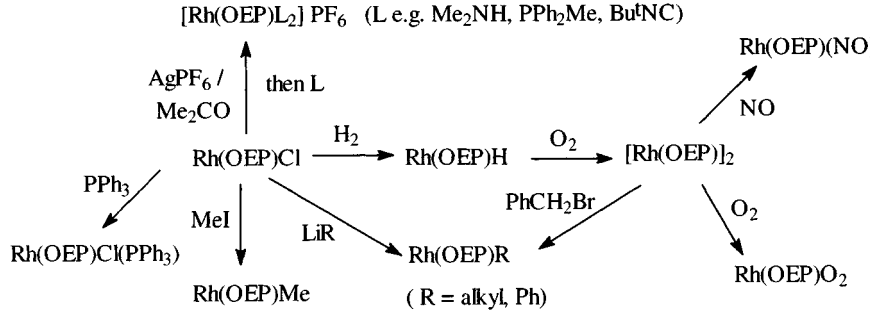

Figure 2.52 Reactions of rhodium porphyrin complexes.

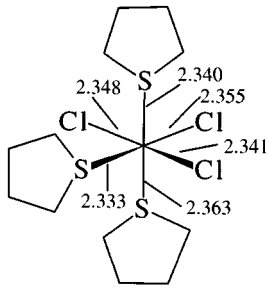

Figure 2.53 Structure of $RhCl_3$(tetrahydrothiophene)$_3$.

Similar reactions with PhSR (R = Me, Et, Pr, Bu) give *mer*-$RhX_3(PhSR)_3$ and some *fac*-isomer for R = Et, Bu. X-ray diffraction confirms (Figure 2.53) the *mer*-structure for the tetrahydrothiophene complex $RhCl_3(C_4H_8S)_3$, which has been used as a convenient starting material for making organorhodium compounds.

^{1}H NMR shows no exchange with added C_4H_8S [104].

Tris-chelates with bidentate S-donors are made conventionally (Rh–S 2.368 Å for $Rh(S_2CNEt_2)_3$)

$$RhCl_3.3H_2O \xrightarrow[H_2O/EtOH\ heat]{NaY} RhY_3 \qquad (Y = S_2CNR_2, S_2P(OEt)_2)$$

On oxidation of $Rh(S_2CNMe_2)_3$, an unusual dimer is formed (Figure 2.54) with different rhodium environments; the $Rh_2(S_2CNMe_2)_5^+$ has no metal–metal bond (Rh–Rh 2.556 Å) [105].

The dithioacetylacetonate is made by preparing the ligand *in situ*; the stable red crystals have 6-coordinate rhodium (Rh–S 2.314–2.333 Å;

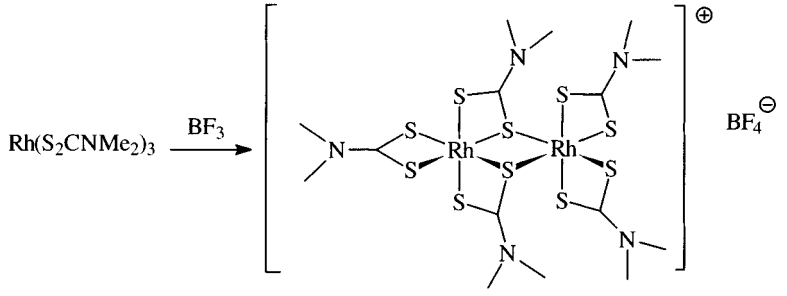

Figure 2.54 Synthesis of $[Rh_2(S_2CNMe_2)_5]^+$.

Table 2.5 Complexes formed by reaction of $RhCl_3$ with tertiary phosphines

Phosphine	Example		Complex formed
Small trialkyl	Me_3P		*fac*- and *mer*-$RhCl_3(PR_3)_3$
Large trialkyl	Bu_3P		*mer*-$RhCl_3(PR_3)_3$
Arylalkyl	Me_2PhP		*mer*-$RhCl_3(PR_3)_3$
Bulky alkyl	Bu^t_2PrP	(cold)	$RhCl_2(PR_3)_2$
	Bu^t_2PrP	(heat)	$RhHCl_2(PR_3)_2$
	Bu^t_3P	(heat)	$RhH_2Cl(PR_3)_2$
Triaryl	Ph_3P	(cold)	$RhCl_3(PR_3)_3$
	Ph_3P	(heat)	$RhCl(PR_3)_3$
	$(o\text{-tolyl})_3P$	(cold)	$RhCl_2(PR_3)_2$

S–Rh–S 97°) in a geometry very similar to the acetylacetonate (section 2.9.1) [106].

$$RhCl_3.3H_2O + MeCOCH_2COMe \xrightarrow[HCl/EtOH,0°C]{H_2S} Rh(MeCSCHCSMe)_3$$

Thiacrown ether and related systems also tend to involve octahedrally coordinated rhodium(III) [107].

2.9.5 Tertiary phosphine complexes

Rhodium(III) forms a wide range of complexes with tertiary phosphines and arsines [108, 109], though in some cases other oxidation states are possible. Table 2.5 summarizes the complexes produced from reaction of $RhCl_3$ with stoichiometric quantities of the phosphine.

Other halides can be introduced by metathesis. Figure 2.55 summarizes some of the complexes isolable with dimethylphenylphosphine, similar in general to the corresponding iridium complexes (section 2.13.3), including the photochemical isomerization of the *mer*-isomer.

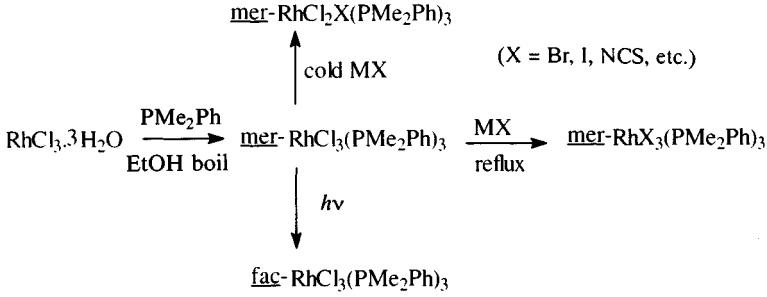

Figure 2.55 Synthesis of rhodium dimethylphenylphosphine complexes.

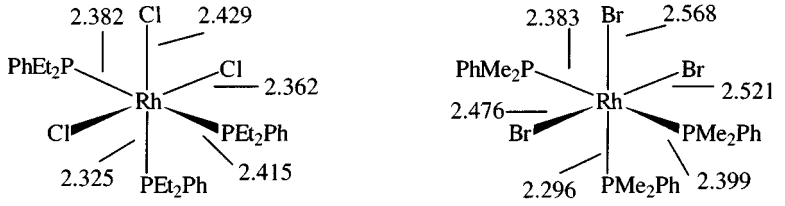

Figure 2.56 Bond lengths in octahedral rhodium(III) complexes of dialkylphenyl phosphines.

Crystal structures have been determined (Figure 2.56) for $RhCl_3(PEt_2Ph)_3$ and $RhBr_3(PMe_2Ph)_3$ (in both cases *mer*-isomer) – in each case, the Rh–X bond length shows the *trans*-influence of a tertiary phosphine [110].

Using less than 3 mol of phosphine affords binuclear complexes $Rh_2Cl_6(PR_3)_n$ ($n = 3, 4$), also obtained by reproportionation (Figure 2.57).

The structures of the two tri(*n*-butyl)phosphine complexes of this type have been determined (Figure 2.58), again showing the high *trans*-influence of PR_3 compared with Cl (Figure 2.58).

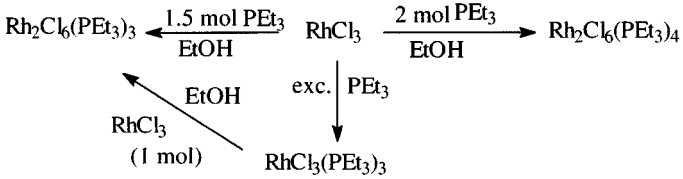

Figure 2.57 Interconversion between rhodium triethylphosphine complexes.

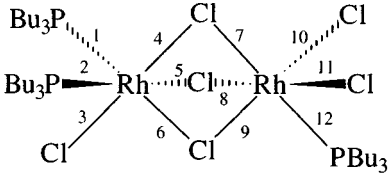

1 = 2.264; 2 = 2.249; 3 = 2.314
4 = 2.362; 5 = 2.504; 6 = 2.462
7 = 2.573; 8 = 2.365; 9 = 2.359
10 = 2.282; 11 = 2.291; 12 = 2.249

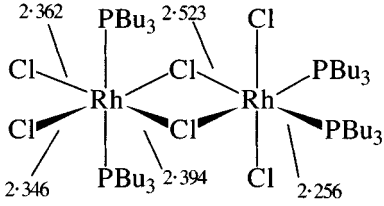

Figure 2.58 Bond lengths in rhodium complexes of tributylphosphines.

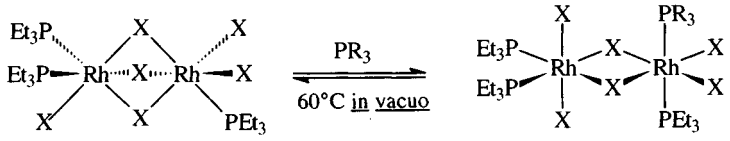

Figure 2.59 Interconversion between dimeric triethylphosphine complexes.

^{31}P NMR shows that when a tertiary phosphine is added to $Rh_2X_6(PEt_3)_3$, one isomer is exclusively produced, the process being reversible (Figure 2.59).

Similarly, adding 2.5 mol PEt_3 to 1 mol of $Rh_2Br_6(PEt_3)_4$ yields exclusively *mer*-$RhBr_3(PEt_3)_3$ [111, 112].

Hydride groups can be introduced by various methods [113], either abstraction of hydrogen from a solvent or a reducing agent, or by oxidative addition:

$$RhCl_3(PMePh_2)_3 \xrightarrow[EtOH]{H_3PO_2} RhHCl_2(PMePh_2)_3$$

$$RhCl_3 \xrightarrow[H_2O/Pr^iCH\ reflux]{PBu^tPr_2} RhHCl_2(PBu^tPr_2)_2$$

$$RhCl(PBu^t_3)_2 \xrightarrow[hexane]{H_2} RhH_2Cl(PBu^t_3)_2$$

Bond lengths in $RhH_2Cl(PBut_3)_2$ are shown in Figure 2.60.

Carbonyl derivatives can be made similarly, either by abstracting CO from the solvent, by direct introduction or by oxidative addition to a Vaska-type complex:

$$RhCl_3 \xrightarrow[EtOH]{PPhEt_2/CO} RhCl_3(CO)(PPh_3)_2$$

$$RhCl(CO)(PPh_3)_2 \xrightarrow{Cl_2} RhCl_3(CO)(PPh_3)_2$$

NMR spectra of $RhX_3(PR_3)_3$ complexes

NMR spectra of tertiary phosphine complexes are often helpful in assigning stereochemistries [114] and two examples of *mer*-isomers are illustrated here.

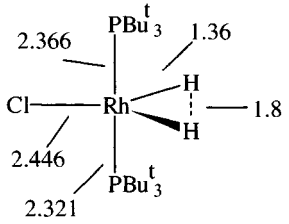

Figure 2.60 Bond lengths in $RhH_2Cl(PBu^t_3)_2$.

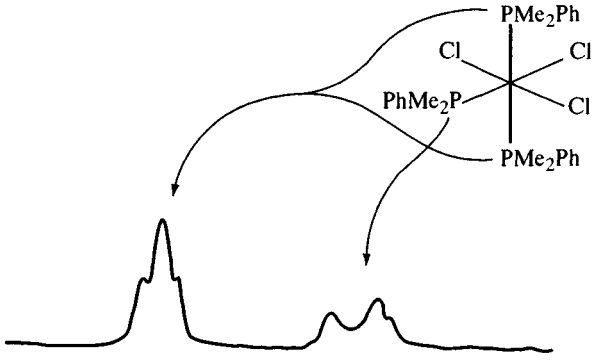

Figure 2.61 The methyl region of the ^{1}H NMR spectrum of *mer*-$RhCl_3(PMe_2Ph)_3$ demonstrating the 'virtual coupling' of the resonances as a result of the mutually *trans*-phosphines. (Reproduced with permission from S.A. Cotton and F.A. Hart, *The Heavy Transition Elements*, published by Macmillan Press Ltd, 1975.)

The methyl region of the ^{1}H NMR spectrum of *mer*-$RhCl_3(PMe_2Ph)_3$ is illustrated in Figure 2.61.

The resonance of the methyl in the unique phosphine is a doublet (splitting owing to coupling with ^{31}P, $I = \frac{1}{2}$), while the corresponding resonance for the methyls in the mutually *trans*-phosphines appears to be a 1 : 2 : 1 triplet. Such a triplet would be expected if the hydrogens were equally coupled to the two phosphorus nuclei – this cannot be the case: (^2J(P–H) could scarcely be the same as ^4J(P–H)). The phenomenon is known as 'virtual coupling' and is commonly found in complexes of PMe_2Ph and certain other methyl-substituted tertiary phosphines, with 4d and 5d metals. (If the case is treated as an $A_3XX'A_3'$ spin system, when $J(X–X)'$ is much larger than J(A–X), a 1 : 2 : 1 triplet obtains with a spacing equal to $1/2J$(A–X). It arises because with heavy metals $J(P–P)_{trans}$ is much greater than $J(P–P)_{cis}$.)

The ^{31}P NMR spectrum of *mer*-$RhCl_3(PMe_3)_3$ is shown in Figure 2.62; again two of the ligands are equivalent, so the spectrum is a doublet for

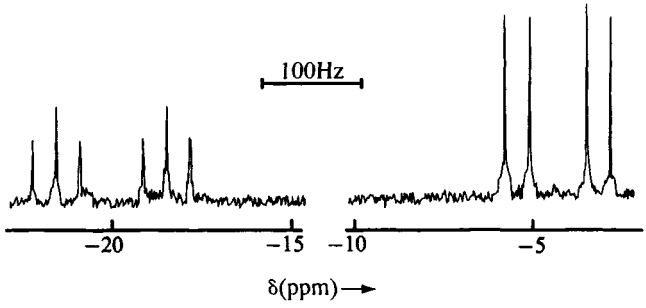

Figure 2.62 The ^{31}P NMR spectrum of *mer*-$RhCl_3(PMe_3)_3$, with random noise decoupling of the protons. (Reproduced with permission from *J. Chem. Soc., Dalton Trans.*, 1973, 704.

the two equivalent phosphines, split by the third, and a triplet for the third phosphine (split by two equivalent P), each signal in turn split by coupling to ^{103}Rh ($I = \frac{1}{2}$). (Doublet $\delta = -20.0$ Hz, $J(Rh-P) = 112.1$ Hz; $J(P-P) = 24.2$ Hz. Triplet $\delta = -4.3$ Hz, $J(Rh-P) = 83.8$ Hz). The ^{31}P NMR of *fac*-$RhCl_3(PEt_3)_3$ where all phosphines are equivalent is a doublet, the only splitting is owing to Rh–P coupling (114 Hz) similar to that found for P *trans* to Cl in the *mer*-isomer.

Case studies of phosphine complexes

An immense number of phosphine complexes of rhodium have been synthesized and detailed compilations of information are available [3d]. In this section, some case studies are presented to illustrate the variations that arise as a result of changes in the steric requirements of the phosphine.

Complexes of trimethylphosphine (cone angle 118°) [115]. Syntheses are shown in Figure 2.63. The rhodium(III) complexes can be made by the usual routes or by oxidation of rhodium(I) complexes. Note that in contrast with the bulkier PPh_3, refluxing $RhCl_3$ with PMe_3 does not result in reduction.

Complexes of triphenyl phosphine (cone angle 145°). Fusing anhydrous $RhCl_3$ with PPh_3 is reported to afford $RhCl_3(PPh_3)_3$, also prepared by chlorine oxidation of $RhCl(PPh_3)_3$. Normally, however, particularly on refluxing with excess PPh_3, reduction occurs and the important rhodium(I)

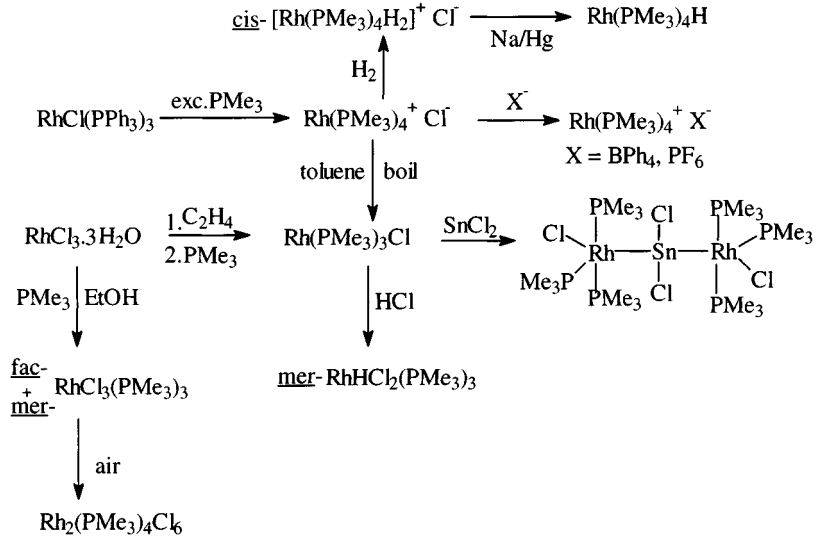

Figure 2.63 Syntheses and interrelationships between rhodium complexes of trimethylphosphine.

complex $RhCl(PPh_3)_3$ is obtained (section 2.7.1). A few other arylphosphines similarly act as reducing agents [45]. Wilkinson's catalyst contains traces of a paramagnetic impurity, long believed to be $RhCl_2(PPh_3)_2$. This has recently been reported as a serendipitous product of the cleavage of a rhodium diene complex, but the preparation has not yet been repeated [116].

Complexes of triisopropylphosphine (cone angle 160°) [69, 117]. In contrast to less bulky trialkylphosphines, a complex $RhCl_3(PPr^i_3)_3$ has only been made by reaction at 0°C: at higher temperatures, hydrides like $RhHCl_2(PPr^i_3)_2$ result (the less bulky tri(*n*-propyl)phosphine gives the 3:1 complex at reflux).

Recently, cleavage of the dimeric cyclooctene complex with PPr^i_3 under either hydrogen or nitrogen has been shown to afford $RhClH_2(PPr^i_3)_2$ and $RhCl(N_2)(PPr^i_3)_2$ (Figure 2.64); these compounds have trigonal bipyramidal and planar structures, respectively.

Controlled chlorination with *N*-chlorosuccinimide results in the formation of square pyramidal $RhHCl_2(PPr^i_3)_2$ and planar $RhCl_2(PPr^i_3)_2$ (Figure 2.65).

Reaction of $RhCl_3$ and sodium amalgam with triisopropylphosphine under a hydrogen atmosphere yields a distorted square planar complex $RhH(PPr^i_3)_3$ (Figure 2.66).

Its structure shows the *trans*-influence of hydride and pronounced distortion from square planar geometry (H–Rh–P 70.7°) owing to steric crowding. ($RhH(PPh_3)_3$ is rather less distorted (H–Rh–P 75.8°) [118a]. This 16-electron complex shows no tendency to add an extra molecule of phosphine, unlike the less hindered $RhH(PEt_3)_3$. It is, however, an active

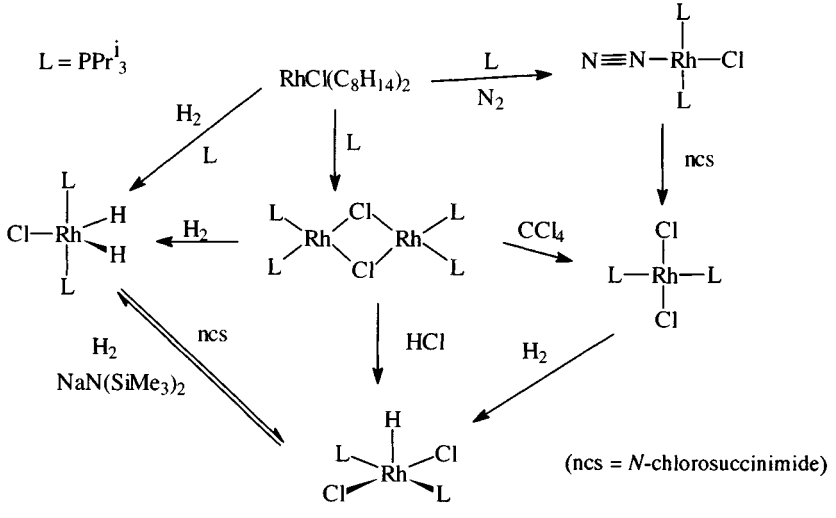

Figure 2.64 Interrelationships between rhodium complexes of triisopropylphosphine.

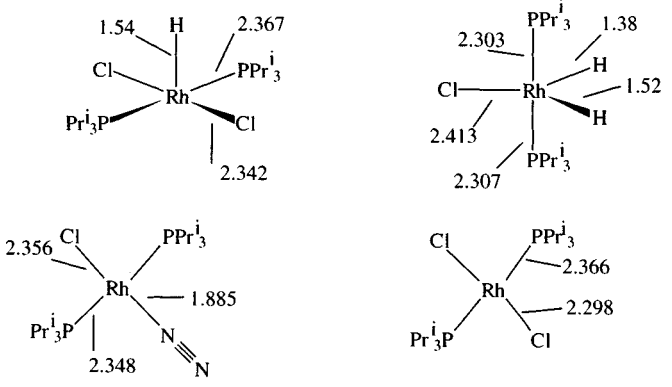

Figure 2.65 Bond lengths in rhodium complexes of triisopropylphosphine.

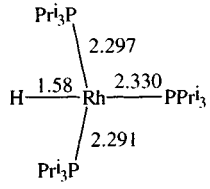

Figure 2.66 Bond lengths in $RhH(PPr^i_3)_3$.

catalyst for the hydrogenation of nitrites – this may result from dissociation to $RhH(PPr^i_3)_2$, as occurs with known $RhH(Pcy_3)_2$. A dimer, $[Rh_2H_4(PPr^i_3)_4]$ is also known [118b], it has the structure $[Pr^i_3P)_2Rh(\mu\text{-}H)_3RhH(PPr^i_3)_2]$.

Complexes of t-*butyl phosphines (PBu$^t_3$ cone angle 182°, PBu$^t_2$Me cone angle 161°)* [119]. Reaction of an excess of bulky trialkylphosphines with $RhCl_3.3H_2O$ does not yield $RhCl_3(PR_3)_3$ species; instead there is reduction to a rhodium(II) species $RhCl_2(PBu^t_2R)_2$ (R = Me, Et, Pr). However, if this synthesis is carried out at elevated temperatures, hydride abstraction occurs to give 5-coordinate $RhHCl_2(PBu^t_2R)_2$ (Figure 2.67); these compounds have NMR hydride signals at unusually high fields ($\delta \sim -30$ ppm). These undergo rapid carbonylation with alcoholic methoxide to give Vaska-type complexes

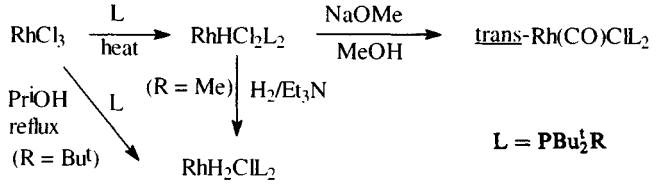

Figure 2.67 Syntheses of rhodium complexes of bulky di(*t*-butyl)alkylphosphines.

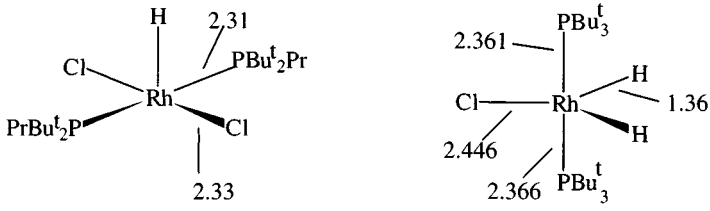

Figure 2.68 Bond lengths in two 5-coordinate rhodium hydride complexes with bulky tertiary phosphines.

(Figure 2.68); while 5-coordinate (tbp) dihydrides have also been synthesized [119b].

The ^{31}P NMR spectrum of $RhH_2Cl(PBu^t_2)_2$ is shown in Figure 2.69; the triplets show coupling with two equivalent hydrogens, split further by coupling with rhodium (J(Rh–P) 110.3 Hz; J(P–H) 14.9 Hz).

2.10 Iridium(I) complexes

Like rhodium(I), the iridium(I) complexes are stabilized by π-bonding ligands such as PR_3 and CO, with 4- and 5-coordinate geometries.

2.10.1 Tertiary phosphine complexes

$IrCl(PPh_3)_3$, the iridium analogue of Wilkinson's compound, illustrates the differences that can arise between two very similar metals. Unlike $RhCl(PPh_3)_3$, it cannot be made by heating $IrCl_3$ with excess phosphine, using the phosphine as a reducing agent, as hydride complexes are formed, a characteristic of iridium. Stable hydrides can also be made by oxidative addition to $IrCl(PPh_3)_3$ (Figure 2.70) [120].

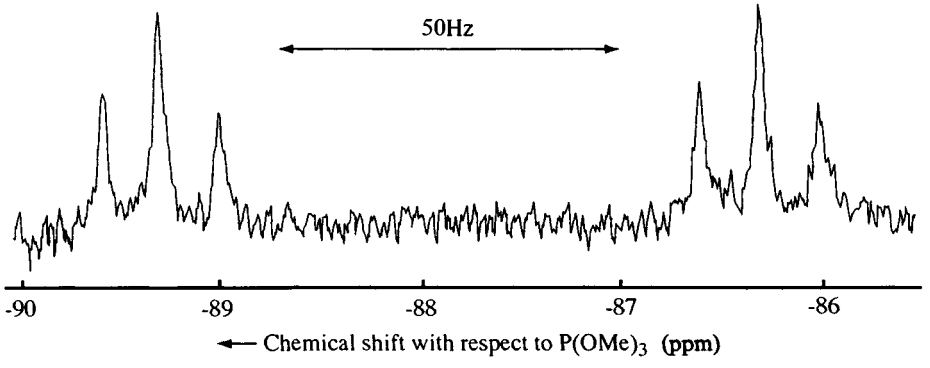

Figure 2.69 The ^{31}P NMR spectrum of $RhH_2Cl(PBu^t_3)_3$, with decoupling of the protons. (Reproduced with permission from *J. Chem. Soc., Series A*, 1971, 3684.)

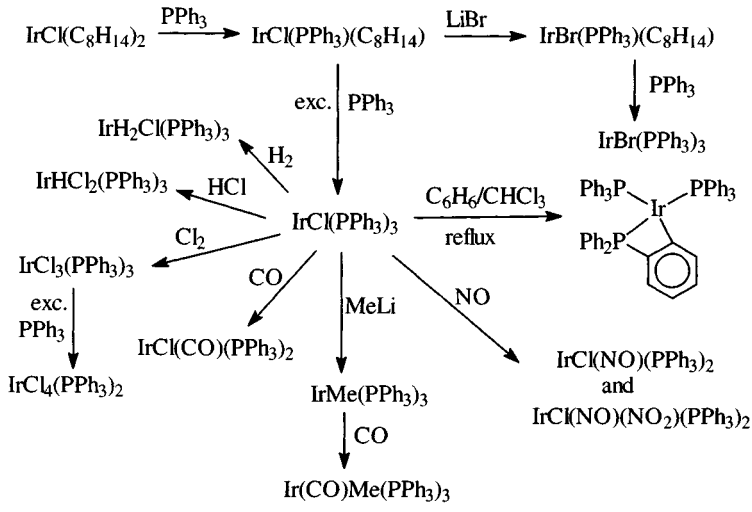

Figure 2.70 Synthesis and reaction of $IrCl(PPh_3)_3$.

$IrCl(PPh_3)_3$, which can be made by displacing alkene from IrCl(cyclooctene)$_2$, does not act as a hydrogenation catalyst for two main reasons: (a) the strong Ir–H bonds do not permit hydride transfer to coordinated alkene; (b) the hydride complexes like $IrH_2Cl(PPh_3)_3$ do not dissociate so there is no vacant coordination site capable of binding an alkene. The iridium methyl shown in Figure 2.70 is unstable to cyclometallation; recent study of the alkyls $Ir(PMe_3)_3(CH_2EMe_3)$ (E = C, Si) shows them to be thermally unstable too, metallating via a 6-coordinate iridium(III) hydride complex without dissociating a phosphine (Figure 2.71) [121].

A number of $Ir(PR_3)_4^+$ complexes exist [122]:

$$IrCl(CO)(PPh_3)_2 \xrightarrow[MeCN]{AgClO_4} Ir(CO)(MeCN)(PPh_3)_2^+$$

$$\xrightarrow[PPh_2Me]{exc.} Ir(PPh_2Me)_4^+ClO_4^-$$

The cation has significant tetrahedral distortion from square planar geometry (P–Ir–P ~150°) to minimize non-bonding interactions. It undergoes various oxidative addition reactions

$$Ir(PPh_2Me)_4^+ \xrightarrow{XY} IrXY(PPh_2Me)_4^+ \qquad (XY = H_2, HCl, Cl_2)$$

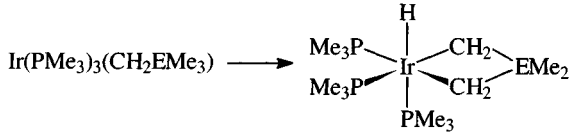

Figure 2.71 Cyclometallation of an iridium neopentyl.

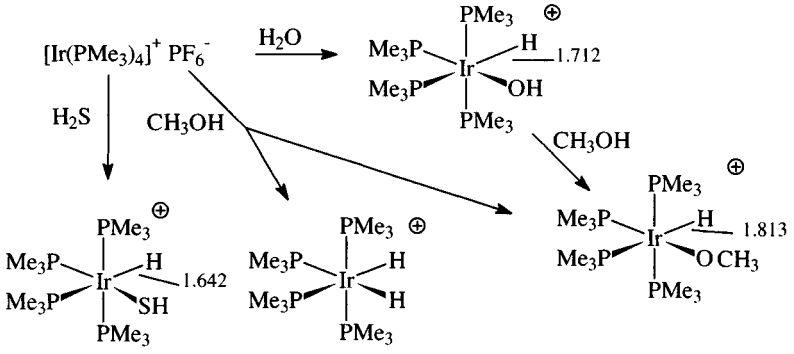

trans-Ligand	Ir—P
OH	2.259
OMe	2.274
SH	2.298
Trimethylphosphine	2.336–2.355
H	2.369–2.378

Figure 2.72 Oxidative additive reactions of $[Ir(PMe_3)_4]^+$ and bond lengths.

The similar species $Ir(PMe_3)_4^+$ likewise shows tetrahedral distortion from square planar geometry (P–Ir–P 152.6–158.9°). It undergoes some remarkable oxidative addition reactions with species like H_2O and H_2S (Figure 2.72).

The Ir–P bond lengths in the complexes allow the ligands to be placed in order of *trans*-influence.

Using the chelating phosphine bis(diphenylphosphino)ethane (dppe) a related complex $Ir(dppe)_2^+$ can be made [123]

$$IrCl(CO)(PPh_3)_2 \xrightarrow[C_6H_6]{dppe} [Ir(dppe)_2CO]^+Cl^-$$

$$\xrightarrow[\text{toluene}]{100°C} Ir(dppe)_2^+Cl^- + CO$$

The orange complex, though quite air stable in the solid state, forms an 'irreversible' dioxygen adduct (IR ν(O–O) 845 cm^{-1}) in solution within a few minutes. The complex likewise adds H_2, HCl, HBr and, reversibly, CO. An adduct with MeNC is formed by a photochemical route:

$$Ir(MeNC)_4^+ \xrightarrow[h\nu]{dppe} Ir(dppe)_2(CNMe)^+$$

The square planar iridium isocyanide complexes [124]

$$IrCl_3 \xrightarrow[150°C]{CO} [IrCl(CO)_3]_x \xrightarrow{RNC} Ir(CNR)_4^+$$

(R, e.g. cyclohexyl, *p*-tolyl) readily undergo oxidative addition with molecules like Cl_2 and MeI to give iridium(III) complexes

$$Ir(CNR)_4^+ + XY \rightarrow IrXY(CNR)_4^+$$

2.10.2 Vaska's compound

The 1961 report that Vaska's compound ($IrCl(CO)(PPh_3)_2$) reversibly binds dioxygen sparked off an intense study of addition reactions of this and related compounds that has continued unabated up to the present day [125].

Vaska's compound may be prepared as yellow air-stable crystals by various reactions, such as conventional substitution

$$IrCl(CO)_3 \xrightarrow{PPh_3} IrCl(CO)(PPh_3)_2 + 2CO$$

or, more usually, by CO abstraction

$$IrCl_3.xH_2O \xrightarrow[MeOCH_2CH_2OH \text{ or DMF}]{PPh_3/\text{reflux}} IrCl(CO)(PPh_3)_2$$

The complex has a *trans*-structure [126] (Figure 2.73).

It undergoes a wide range of addition reactions with molecules XY:

$$IrCl(CO)(PPh_3)_2 + XY \rightarrow IrClXY(CO)(PPh_3)_2$$

If X–Y bond fission occurs, the product is a 6-coordinate iridium(III) complex (Table 2.6); otherwise a 5-coordinate (or pseudo-5-coordinate) adduct is obtained in which Ir formally retains the (+1) state (Table 2.7). This distinction can be somewhat artificial; $IrCl(O_2)CO(PPh_3)_2$ can be regarded as an iridium(III) peroxo complex.

Solutions of Vaska's compound react with oxygen to form $IrCl(O_2)(CO)(PPh_3)_2$; the dioxygen molecule can be removed by heating the solid *in vacuo* to 100°C or by simply flushing the solution with nitrogen. Under the same conditions, it reacts with hydrogen forming the stable octahedral complex $IrClH_2(CO)(PPh_3)_2$; CO is reversibly absorbed as $IrCl(CO)_2(PPh_3)_2$ while SO_2 forms a stable (but reversible) adduct $IrCl(SO_2)(CO)(PPh_3)_2$, where the SO_2 is bound to iridium by sulphur. An indication of the bond strength in the SO_2 adduct, about 40 kJ mol^{-1}, has been obtained by differential scanning calorimetry (a second molecule of SO_2 can be bound, probably via an Ir–Cl → SO_2 linkage).

Adduct formation by $IrCl(CO)(PPh_3)_2$ and similar compounds results in a shift in the IR carbonyl stretching frequency (Table 2.8).

With the exception of the CO adduct, as might be expected, the adducts have higher stretching frequencies. The largest values are found for the 'irreversible' adducts with the halogens, corresponding to the higher positive charge on the metal. Therefore, as electrons are removed from the metal in

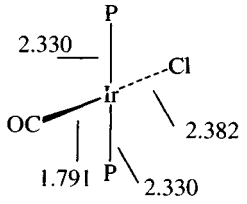

P—Ir—P 180°
Cl—Ir—C 178°

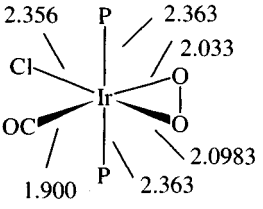

P—Ir—P 174.5°
Cl—Ir—C 97°
O—Ir—O 41.8°

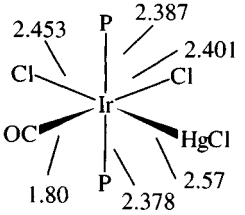

P—Ir—P 175.3°
Cl—Ir—C 171.1°
Cl—Ir—Hg 176.9°

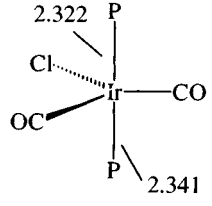

P—Ir—P 176.8°
Cl—Ir—C 118.2–120.9°

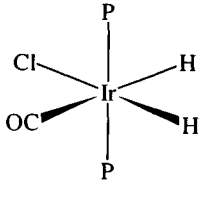

P—Ir—P ≈ 180°
Cl—Ir—C ≈ 90°

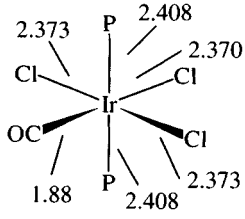

P—Ir—P 179°
Cl—Ir—C 87.6° (cis)

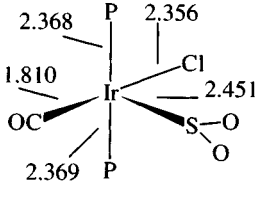

P—Ir—P 167.9°
Cl—Ir—C 171°

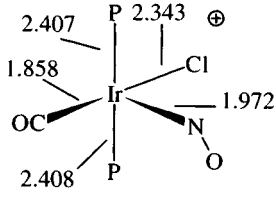

P—Ir—P ≈ 175.7°
Cl—Ir—C ≈ 161.3°

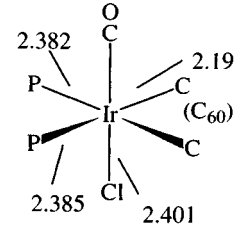

P—Ir—P 1139°
Cl—Ir—C 179.6° (cis)
C—Ir—C 41°

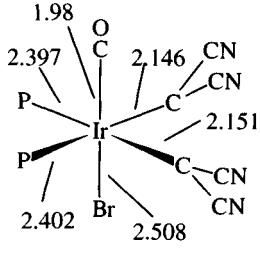

(P = PPh_3)

P—Ir—P 110°
Cl—Ir—Br ≈ 180°
(NC)C—Ir—C(CN) 41°

Figure 2.73 Structural data for Vaska's compound and its adducts.

Table 2.6 Formation of 6-coordinate products from Vaska's compound

Reactant	Product
H_2	$IrClH_2(CO)(PPh_3)_2$
HCl	$IrCl_2H(CO)(PPh_3)_2$
Cl_2	$IrCl_3(CO)(PPh_3)_2$
$HgCl_2$	$IrCl_2(HgCl)(CO)(PPh_3)_2$
$SiHCl_3$	$IrClH(SiCl_3)(CO)(PPh_3)_2$
$SiEtHCl_2$	$IrClEt(SiHCl_2)(CO)(PPh_3)_2$
MeI	$IrClMeI(CO)(PPh_3)$
Cl_2S	$IrCl_2(SCl)(CO)(PPh_3)_2$
SiH_3Cl	$IrCl_2(SiH_3)(CO)(PPh_3)_2$
$S(CN)_2$	$IrCl(NCS)CN(CO)(PPh_3)_2$
HCN	$IrClH(CN)(CO)(PPh_3)_2$

Table 2.7 Formation of 5-coordinate (or pseudo-5-coordinate) products from Vaska's compound

Reactant	Product
O_2	$IrCl(O_2)(CO)(PPh_3)_2$
CO	$IrCl(CO)_2(PPh_3)_2$
SO_2	$IrCl(SO_2)(CO)(PPh_3)_2$
BF_3	$IrCl(BF_3)(CO)(PPh_3)_2$
$(NC)_2C{=}C(CN)_2$	$IrCl[(NC)_2C_2(CN_2)](CO)(PPh_3)_2$
$RC{\equiv}CR$	$IrCl(RCCR)(CO)(PPh_3)_2$
C_2F_4	$IrCl(F_2CCF_2)(CO)(PPh_3)_2$
N_2H_4/PPh_3	$IrH(CO)(PPh_3)_3$
$PhCON_3$	$IrCl(N_2)(PPh_3)_2$
C_n ($n = 60, 70$)	$IrCl(C_n)(CO)(PPh_3)_2$

Table 2.8 IR data for adducts of $IrCl(CO)(PPh_3)_2$

Molecule added	ν(CO) (cm^{-1})[a]
–	1967
O_2	2015
SO_2	2021
BF_3	2067 (C_6H_6)
HCl	2046
MeI	2047
C_2F_4	2052
$(NC)_2C{=}C(CN)_2$	2057
I_2	2067
Br_2	2072
Cl_2	2075
D_2	2034
CO	1934, 1988
C_{60}	2014 (mull)
C_{70}	2002 (sh 2012) (mull)

[a] Solution in $CHCl_3$ unless noted.

forming the adduct, the ability of the metal to participate in back-donation to the anti-bonding CO π^*-orbitals is reduced; as a result, the CO bond order increases.

Structures of some adducts [127] together with the parent compound are shown in Figure 2.73. If oxygen is treated as a monodentate ligand, then the structure of the oxygen adduct can be called trigonal bipyramidal similar to the CO adduct. The PPh_3 groups adopt *trans*-positions, favoured on steric grounds, which are also formed in the adducts with the halogens and $HgCl_2$. When the bulkier groups such as $(NC)_2C{=}C(CN)_2$ or C_n ($n = 60$, 70, 84) bind to iridium, the halogen and carbonyl groups occupy the 'axial' positions, as axial phosphines would involve non-bonding interactions with the bulky electron donors. Study of the structural data in Figure 2.73 shows a tendency for bond length to increase upon adduct formation though the more ionic Ir–Cl bonds seem to be less affected.

The structures of several adducts can be rationalized on the basis [128] that in a 5-coordinate low-spin d^8 tbp system, the acceptor ligands prefer to occupy an equatorial site ($IrCl(CO)_2(PPh_3)_2$) whereas a π-donor prefers an axial site. In a square pyramidal situation, it is weakly bonded acceptors that prefer the apical position, e.g. $(IrCl(SO_2)(CO)(PPh_3)_2$.

Some syntheses for other $IrX(CO)(PPh_3)_2$ complexes follow:

$$IrCl(CO)(PPh_3)_2 \xrightarrow[MeCN]{AgClO_4} Ir(MeCN)(CO)(PPh_3)_2^+ \xrightarrow{X^-} IrX(CO)(PPh_3)_2 \quad (X = Br, I, CN, NCS, CNO, OH)$$

$$IrCl(CO)(PPh_3)_2 \xrightarrow[Ag_2CO_3]{NH_4F} IrF(CO)(PPh_3)_2$$

$$IrCl(CO)(PPh_3)_2 \xrightarrow{NaOR} Ir(OR)(CO)(PPh_3)_2 \quad (R = Me, Ph, Bu^t, C_6F_5)$$

$$IrCl(CO)(PPh_3)_2 \xrightarrow{MeLi} Ir(Me)(CO)(PPh_3)_2$$

The most versatile route involves the synthesis of the MeCN complex; the weakly bound nitrite is readily replaced by a variety of anions. These generally react in a similar way to the chloride, IR data for these and their dioxygen adducts are given in Table 2.9 [129].

Structures for a number of *trans*-$IrX(CO)(PR_3)_2$ systems have been determined (Table 2.10).

The Ir–P bonds show little dependence upon the *cis*-ligand X, as expected [130].

Complexes with other phosphines can be prepared by the general route of refluxing $IrCl_3$ or $IrCl_6^{2-}$ in an alcohol that acts as the source of CO, then adding the phosphine. In certain cases, a displacement reaction can be used

$$IrCl(CO)(PPh_3)_2 + 2PMe_3 \rightarrow IrCl(CO)(PMe_3)_2 + 2PPh_3$$

Table 2.9 IR data for $IrX(CO)(PPh_3)_2$ and its O_2 adducts (cm^{-1})

X	ν(CO)[a]		O_2 adduct		
	Mull	Solution	ν(CO) (mull)	ν(O–O) (mull)	Rev/irrev[b]
F	1944	1957	2005	850	
Cl	1960	1965	2005	855	rev
Br	1955	1966		862	rev
I	1975	1967	2005	850	irrev
OH	1930, 1950	1949			
Me	1935 (KBr)	1937 (C_6H_6)	1967	827	irrev
NCS	1970	1976	2015	855	rev
SH	1945	1965 (KBr)	1960	845	irrev
C_6F_5	1965 (KBr)	1990	no adduct		
NCO	1965	1968	2010	855	rev
C≡CPh	1955	1955 (CH_2Cl_2)	1990	835	irrev
SPh		1950			
CN		1990			
NCSe		1987			

[a] Solution in $CHCl_3$ unless noted; [b] Reversible or irreversible.

IR data [131] shows a trend to increasing ν(C–O) as the substituents on the phosphine became more electron withdrawing (Table 2.11) so that as the σ-donor power of the phosphine decreases and the π-acceptor power increases, the electron density at Ir decreases and electrons are removed from the π^*-orbital of CO [132].

There is a similar trend relating ν(C–O) to the π-acceptor strength of X (Figure 2.74).

The stereochemistry and mechanism of oxidative addition

In general when a molecule AB adds to a complex $IrX(CO)L_2$ [10, 133], second-order kinetics are exhibited

$$\text{rate} = k[\text{Ir complex}][\text{AB}]$$

Table 2.10 Bond lengths in *trans*-$IrX(CO)(PR_3)_2$ (Å)

PR_3	X	Ir–C	Ir–P	Ir–X
PPh_3	Cl	1.791	2.330	2.382
P(*o*-tolyl)$_3$	Cl[a]	1.67	2.338	2.43
P(*o*-tolyl)$_3$	Cl	1.817	2.331	2.364
Pcy_3	Cl	1.808	2.339	2.398
PPh_3	OPh	1.795	2.328, 2.344	2.049
PPh_3	Me[a]	1.835	2.300	2.17
P(*p*-tolyl)$_3$	Me	1.867	2.302, 2.305	2.206
PPh_3	OH	1.797	2.312, 2.314	2.110
PPh_3	C_6F_5	1.891	2.305, 2.326	2.090
PPh_3	OC_6F_5	1.798	2.320, 2.321	2.058
PPh_3	$C_6H_2Me_3$	1.848	2.313, 2.319	2.143

[a] Disordered structure, accuracy limited.

Table 2.11 IR data for $IrCl(CO)(PR_3)_2$ (cm^{-1})

PR_3	ν(CO)		
	Toluene	$CHCl_3$	Mull
Pcy_3	1932	1927	1931
PPr^i_3	1935	1933	
PBu_3	1940	1943	
$PBuPh_2$	1955	1949	
PBz_3	1956	1956	
P(*p*-tolyl)$_3$	1963	1964	
PPh_3	1967	1971	1960
$P(OPh)_3$	2001	2003	
P(*o*-tolyl)		1960	
PMe_3			1938
$AsPh_3$			1958
PBu^t_3	1920[a]		1916

[a] Solution in pentane.

The reaction rates depend on several factors: the halide X, ligand L, even the solvent. Therefore, when MeI adds to $IrX(CO)(PPh_3)_2$ the rate increases in the order I < Br < Cl whereas for the addition of H_2 or O_2, the relative order is reversed.

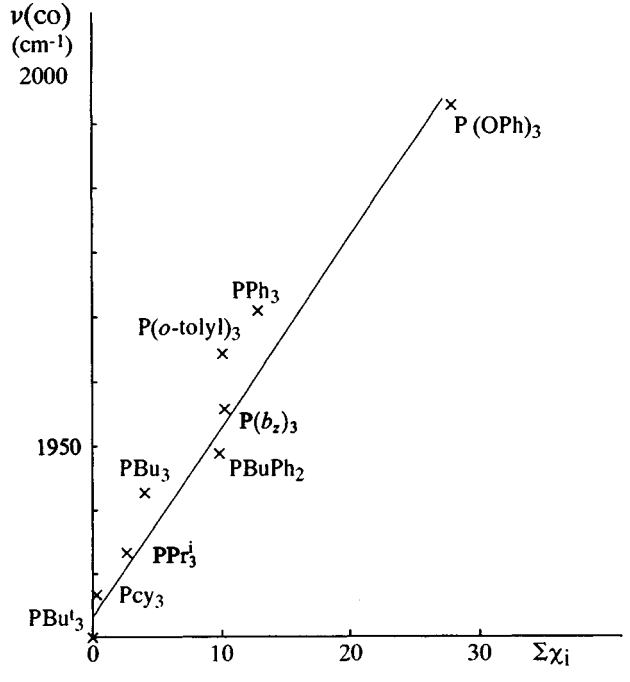

Figure 2.74 Relationship between ν(C–O) for *trans*-$IrCl(CO)(PPh_3)_2$ (in $CHCl_3$ solution) and $\sum \chi_i$ (Tolman's additivity substituent contribution for electronic effects in R_3P). (See *Chem. Rev.*, 1977, **77**, 313.)

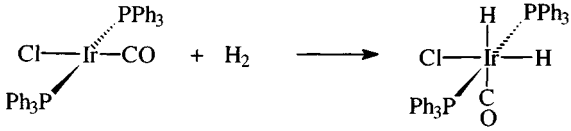

Figure 2.75 Oxidative addition of dihydrogen to Vaska's compound.

No single mechanism accounts for all the reactions. One pathway involves a concerted one-step process involving a cyclic transition state. This of necessity affords a *cis*-product. Another possibility, more favoured in polar solvents, involves a cationic 5-coordinate intermediate $[IrX(A)(CO)L_2]^+$, which undergoes subsequent nucleophilic attack by B^-. Other possibilities include a S_N2 route, where the metal polarizes AB before generating the nucleophile, and radical routes. Studies are complicated by the fact that the thermodynamically more stable isolated product may not be the same as the 'kinetic product' formed by initial addition.

When the adding species AB retains an A–B bond after addition (e.g. O_2), addition is necessarily *cis*. This is also the case when H_2 adds (Figure 2.75); the stereochemistry of this addition keeps the bulky tertiary phosphines apart.

Additionally, MO calculations indicate the lowest energy orientation occurs with the three strongest *trans*-influence ligands (two hydrides and a PPh_3) in a facial configuration. Calculations on compounds $IrX(CO)(PR_3)_2$ indicates that weak donors X and strong π-acceptors PR_3 favour addition in the XIrCO plane [134, 135].

When H_2 adds to *cis*-IrCl(CO)(dppe) (Figure 2.76), two pathways are found [136, 137].

The first product is formed in high yield at low temperatures but subsequently equilibrates with the thermodynamically more stable second product. The direction of the initial addition of H_2 in the P–Ir–CO plane is ascribed to the electron-withdrawing influence of the carbonyl group.

Using more basic (electron-donating) ligands generally speeds up the reactions while bulky ligands slow it down. The use of tris(*o*-tolyl)phosphine is an extreme example of the latter as $IrCl(CO)[P(o\text{-tolyl})_3]_2$ fails to add O_2, H_2 or SO_2 and only adds HCl slowly; the reason is that methyls in an *ortho*-position tend to 'block' the axial positions (Figure 2.77) [126b].

Different results can be found in the solid state and solution; gaseous HX (X= halide) adds *cis* to solid $IrCl(CO)(PPh_3)_2$ and in benzene solution, but in polar solvents like methanol a mixture of *cis*- and *trans*-products is found.

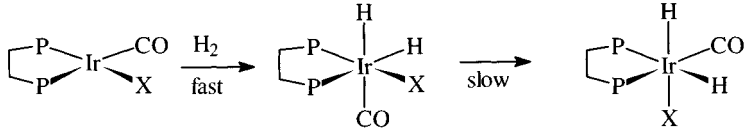

Figure 2.76 Oxidative addition to *cis*-Ir(CO)Cl(dppe).

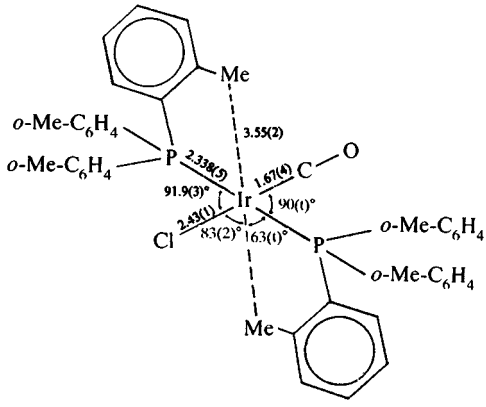

Figure 2.77 The structure of $IrCl(CO)[P(o\text{-tolyl})_3]_2$. (Reprinted with permission from *Inorg. Chem.*, 1975, **14**, 2669. Copyright (1975) American Chemical Society.)

2.11 Dioxygen complexes

Discovery of the ability of $IrCl(CO)(PPh_3)_2$ reversibly to bind dioxygen prompted considerable synthetic and structural study of dioxygen complexes [138]. Early reports of the structures of $IrX(CO)(O_2)(PPh_3)_2$ (X = Cl, Br, I) gave O–O distances of 1.30, 1.36 and 1.509 Å, respectively, compared with 1.21 Å in O_2^{2-}; since the first two were 'reversible' and the iodide an 'irreversible' adduct, it was postulated that the O–O distance correlated with this. Therefore, if electron transfer occurred from non-bonding metal d orbitals to anti-bonding orbitals of O_2, the O–O distance increased with electron donation (with the benefit of hindsight, the insensitivity of ν(O–O) in the IR spectrum contrasted strongly with the apparent variation in the O–O distance). Subsequently, increased structural data (see Table 2.12) indicated that O–O distances fell into a narrower range of 1.41–1.52 Å. It is now believed that some of the earlier studies gave anomalous results because of disorder in the crystal (and possible decomposition).

The presently accepted model for bonding in these dioxygen complexes regards them as essentially peroxo complexes. This view is supported [139] by the similarity in O–O distance to that in O_2^{2-}; likewise the similarity in ν(O–O) in the IR spectrum (Table 2.9) to that in H_2O_2 (880 cm^{-1}), Na_2O_2 (880 cm^{-1}) and $Na_2O_2.8H_2O$ (843 cm^{-1}). ^{17}O NQR studies on $IrCl(CO)O_2(PPh_3)_2$ show resonances at similar frequencies to H_2O_2 [140]. MO calculations suggest that the O_2 ligand donates about 0.1 electron from its $1\sigma_g$ -orbital and 0.2 electron from its π-orbital and accepts around 1.2 electrons from the metal dπ-orbital into its π_g-orbital. This back donation is primarily responsible for weakening the O–O bond [141].

Table 2.12 Bond lengths in dioxygen complexes (Å)

	d(O–O)
$[IrCl(CO)O_2(PPh_2Et)_2]^-$	1.469
$[IrO_2(PMe_2Ph)_4]^+BPh_4^-$	1.49
$[RhO_2(PMe_2Ph)_4]^+BPh_4^-$	1.43
$[RhO_2(AsMe_2Ph)_4]^+ClO_4^-$	1.46
$[IrO_2(Ph_2PCH_2PPh_2)_2]^+ClO_4^-$	1.486
$[IrO_2(Ph_2PCH_2PPh_2)_2]^+PF_6^-$	1.453
$[IrO_2(Ph_2PCH_2CH_2PPh_2)_2]^+PF_6^-$	1.52
$[IrO_2(Ph_2PCH_2PPh_2)_2]^+C(CN)_3^-$	1.39–1.43

The structural changes occurring upon oxygenation can be seen by comparison of the structures of $IrCl(CO)(PPh_3)_2$ and $IrCl(CO)(O_2)(PPh_2Et)_2$ (Figure 2.78); the latter is a more accurate determination than the disordered PPh_3 analogue. The former is essentially square planar, with virtually linear P–Ir–P and Cl–Ir–C geometries.

On reaction with O_2, the P–Ir–P colinearity is maintained (174.5°), keeping these bulky ligands apart, but the Cl–Ir–C angle closes (to 97.4°) to accommodate the incoming O_2 molecule. The geometry of the O_2 adduct can be described as distorted octahedral, with Ir, Cl, C and the two O atoms essentially coplanar. As expected as the coordination number increases, there is a general increase in bond length (except for Ir–Cl).

The S_2 and Se_2 groups are stabilized by bonding to iridium (and rhodium) [142]

$$Ir(dppe)_2Cl + \tfrac{1}{4}Y_8 \xrightarrow{CH_2Cl_2} [Ir(dppe)_2(Y_2)]^+Cl^- \qquad (Y = S, Se)$$

The S–S distance increases from 1.899 Å in S_8 to 2.066 Å (Figure 2.79).

The S_2 group is removed by Hg or R_3P, oxidized by periodate to coordinated S_2O or SO and methylated by Me_3SO_3F.

Iridium(I) can stabilize unusual species like CS, and SO, as well as N_2. The dinitrogen analogue of Vaska's compound is conveniently made as shown in Figure 2.80 [143].

It is essential that reagent grade $CHCl_3$ is used in the synthesis as the trace of ethanol 'stabilizer' removes the aryl isocyanate byproduct and prevents it

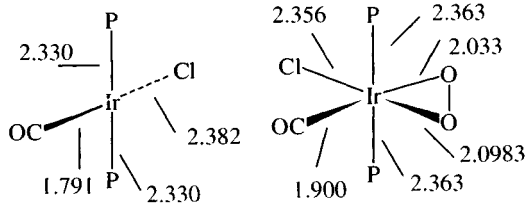

Figure 2.78 A comparison of the structures of $IrCl(CO)(PPh_3)_2$ and $IrCl(CO)O_2(PPh_2Et)_2$.

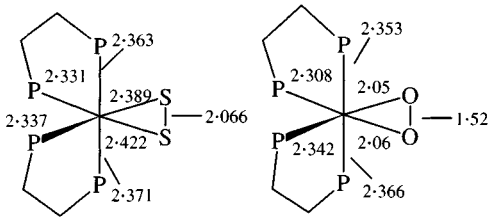

Figure 2.79 A comparison of bond lengths in *cis*-$[Ir(dppe)_2X_2]^+$.

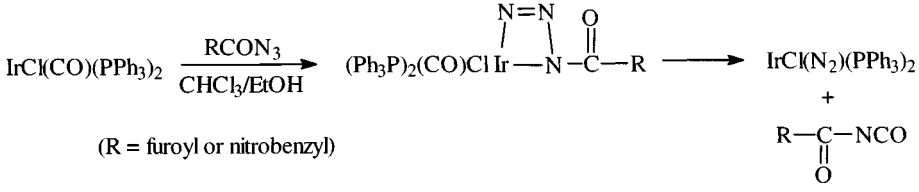

Figure 2.80 Synthesis of the dinitrogen complex $IrCl(N_2)(PPh_3)_2$.

reacting with the dinitrogen complex. The yellow N_2 complex (IR ν(N≡N) 2105 cm^{-1}) is thermally stable but the N_2 ligand is labile and readily replaced by other ligands (Figure 2.81).

The orange thiocarbonyl is air stable (IR ν(C=S) 1332 cm^{-1}); its synthesis proceeds via an isolable C_2S_5 complex that is desulphurized by refluxing with PPh_3 [144]:

$$IrCl(N_2)(PPh_3)_2 \xrightarrow{CS_2} IrCl(C_2S_5)(PPh_3)_2$$

$$\xrightarrow{PPh_3} IrCl(CS)(PPh_3)_2 + Ph_3PS$$

A green–black SO complex (dec. 155°C) with a bent Ir–S–O linkage has been synthesized (Figure 2.82) [145].

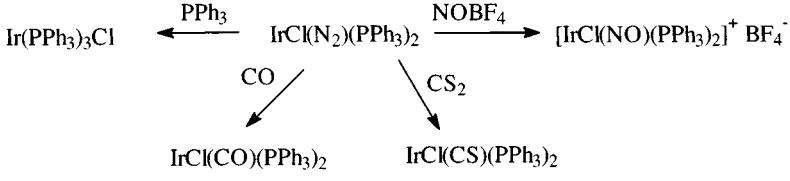

Figure 2.81 Reactions of the dinitrogen complex $IrCl(N_2)(PPh_3)_2$.

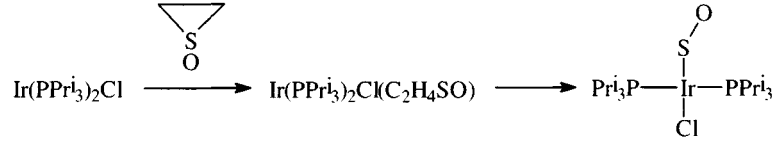

Figure 2.82 Synthesis of an SO complex.

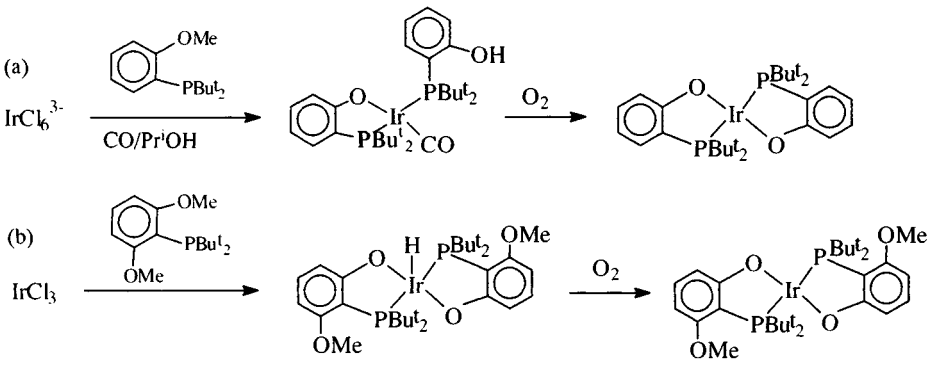

Figure 2.83 Syntheses of iridium(II) phosphine complexes.

2.12 Iridium(II) complexes

The iridium(II) complexes are rarer that those of rhodium(II). Iridium does not seem to form carboxylates $Ir_2(O_2CR)_4$ with the 'lantern' structure; complexes analogous to *trans*-$RhX_2(PR_3)_2$ are not formed with bulky tertiary phosphines, probably because the greater strength of Ir–H bonds leads to $IrHX_2(PR_3)_2$.

The best characterized complexes [146] are prepared as shown in Figure 2.83. In synthesis (a) the first step involves demethylation of both ligands; only one phosphine chelates, demonstrating the stability of square planar d^8 iridium(I); on oxidation, the CO is displaced (as CO_2) and both ligands chelate.

In synthesis (b), the initial product is a 5-coordinate (sp) iridium(III) hydride complex, which is rapidly oxidized in solution to the planar iridium(II) complex. Both of the compounds are paramagnetic with one unpaired electron, as expected for square planar d^7 complexes.

The square planar ion $[Ir(C_6Cl_5)_4]^{2-}$ also contains iridium(II) [147].

2.13 Iridium(III) complexes

A wide range of iridium complexes are formed in the +3 oxidation state, the most important for iridium, with a variety of ligands. The vast majority have octahedral coordination of iridium.

The aqua ion $Ir(H_2O)_6^{3+}$ and halide complexes IrX_6^{3-} have already been mentioned above. The kinetic inertness of the low spin d^6 complexes means that hydrolysis of $IrCl_6^{3-}$ is slow: complexes up to $IrCl_2(H_2O)_4^+$ have been produced and separated from mixtures by high-voltage electrophoresis.

Next Page